Catal Lett (2008) 120:166–178
DOI 10.1007/s10562-007-9297-0

Low Temperature Water–Gas Shift: Alkali Doping to Facilitate Formate C–H Bond Cleaving over Pt/Ceria Catalysts—An Optimization Problem

Harold N. Evin · Gary Jacobs · Javier Ruiz-Martinez · Gerald A. Thomas · Burtron H. Davis

Received: 16 July 2007 / Accepted: 2 October 2007 / Published online: 23 October 2007

Abstract Doping Pt/ceria catalysts with alkali metals was found to lead to an important weakening of the formate C–H bond, as demonstrated by a shift to lower wavenumbers of the ν(CH) vibrational mode. However, with high alkalinity ($\sim$2.5%Na or equimolar amounts of K, Rb, or Cs), a tradeoff was observed such that while the formate became more reactive, the stability of the carbonate species, which arises from the formate decomposition, was found to increase. This was observed by TPD-MS measurements of the adsorbed CO_2 probe molecule. Increasing the amount of alkali to levels that were too high also led to lower catalyst BET surface area, the blocking of the Pt surface sites as observed in infrared measurements, and also a shift to higher temperature of the surface shell reduction step of ceria during TPR. When the alkalinity was too high, the CO conversion rate during water–gas shift decreased in comparison with the undoped Pt/ceria catalyst. However, at lower levels of alkali, the above-mentioned inhibiting factors on the water–gas shift rate were alleviated such that the weakening of the formate C–H bond could be utilized to improve the overall turnover efficiency during the water–gas shift cycle. This was demonstrated at 0.5%Na (or equimolar equivalent levels of K) doping levels. Not only was the formate turnover rate found to increase significantly during both transient and steady state DRIFTS tests, but this effect was accompanied by a notable increase in the CO conversion rate during low temperature water–gas shift.

Keywords Water gas shift · Low temperature water–gas shift · WGS · LTS · Fuel processor · Platinum · Pt · Ceria · Ce · Alkali · Dopants · Electronic effect · Lithium · Li · Sodium · Na · Potassium · K · Rubidium · Rb · Cesium · Cs

1 Introduction

Alkali dopants have long been used to promote water–gas shift activity over metal/oxide heterogeneous catalysts [1–19]. In 1980, Sato and White [1] studied water–gas shift in continuing their work on the application of Pt/TiO_2 catalysts to take advantage of the semiconducting property of titania to spatially separate electrons from holes, such that they could be used in oxidation-reduction reactions. They demonstrated that the water–gas shift reaction could even be carried out at room temperature. The TiO_2 utilized was anatase, and the Pt was loaded to 2%. Under dark conditions, the rate was very slow. However, under illumination, with 0.6 Torr of CO, 2 h were required to achieve 0.6 Torr of H_2 by WGS. In 1981, based on an earlier report by Wagner and Somorjai [2], who indicated that NaOH coating improved liquid photolysis rates over $Pt/SrTiO_3$, Sato and White [3] added a NaOH coating to Pt/TiO_2, and found an improvement in the photocatalyzed water–gas shift rate. With 7% by weight added NaOH, the time to achieve complete CO conversion was cut in half (about 60 min).

Guidelines for the preparation of Cu and Zn bifunctional catalysts were presented by Klier [4, 5]. Klier focused primarily on methods to interdisperse the copper with the

H. N. Evin · G. Jacobs · G. A. Thomas · B. H. Davis (✉)
Center for Applied Energy Research, 2540 Research Park Drive, Lexington, KY 40511, USA
e-mail: davis@caer.uky.edu

J. Ruiz-Martinez
Laboratorio de Materiales Avanzados, Departamento de Química Inorgánica, Universidad de Alicante, Apartado 99, 03080 Alicante, Spain

oxide phase in order to guarantee a small Cu cluster size, for example via the precipitation, decomposition, and reduction of hydroxycarbonate precursors of either Cu/Zn or Cu/Zn/oxide [e.g., $(Cu/Zn)_5(CO_3)_2(OH)_6$]. However, Klier [4, 5] also highlighted the promoting influence of alkali dopants, where Cs > Rb > K > Na, Li. In this case, Klier suggested that the alkali should be present at concentrations less than a monolayer in order to continue to allow the hydrogen transfer reactions to take place, while the basic function of the alkali could also influence the concerted surface mechanism.

Campbell and coworkers [6] investigated the promoting impact of Cs on the water–gas shift rate of Cu based catalysts that was observed by Klier and coworkers [4, 5]. While Klier and coworkers [4, 5] observed a doubling of the water–gas shift rate on high surface area Cu/ZnO catalysts, Campbell et al. [6] observed a much greater promotion of 15 for Cu(111). Cs addition was suggested to assist in dissociating H_2O, their proposed rate limiting step. They indicated that dissociative adsorption of H_2O is important for either a formate or redox mechanism, and therefore, the explanation for Cs promotion can influence either mechanism.

Later, Campbell and coworkers [7] offered a very different explanation for the promoting effect of Cs in studies over Cu(110). They observed an optimum promotion when one Cs atom per 4 Cu atoms was utilized, increasing the water–gas shift rate by a factor of 5. Interestingly, however, in contrast to their earlier view, $Cs_{1.5–2.0}CO_3$ was found after surface analysis (TDS, XPS, AES). In kinetic studies, again using a low H_2O/CO ratio with 10 Torr H_2O and 26 Torr CO, they found that while previously the reaction rate was first order in H_2O and zero order in CO, on the optimally Cs-promoted surface, the reactant orders changed considerably to zero order in H_2O and 0.5 order on CO, suggesting that dissociative adsorption of H_2O was no longer the rate limiting step. The activation energy was found to be 11 kcal/mol on Cs-doped Cu(110) relative to the value of 10 kcal/mol on the undoped Cu(110) surface. They proposed a redox mechanism to describe the catalysis of both the clean and Cs doped surfaces, with Cs playing a role of O mediator among CO_2, H_2O, and CO, where Cs is primarily in the form of carbonate.

Basinska and Domka [8, 9] showed that addition of most alkali metals (Na, and especially K, Rb, or Cs) to Ru promoted α- and δ-Fe_2O_3 led to remarkable improvements in the water–gas shift rates. The loading of Ru was 0.5% and the Group I metal/Ru atomic ratio was 1:1. Jozwiak and coworkers [10] explored the reducibility of Fe oxide, Ru/Fe oxide, and Na promoted Ru/Fe oxide catalysts by TPR (H_2 and CO), TPO, TGA-MS, IR, and XRD. Their measurements confirmed that reduction of iron oxide proceeds via the steps: $3Fe_2O_3$ to 2 Fe_3O_4 to 6 FeO to 6 Fe. The authors linked the water–gas shift activity to the reduction of Fe_3O_4 to Fe_2O_3, and found that both Ru and Na facilitate the reduction step to lower temperature.

Luukkanen and coworkers [11, 12] heterogenized polypyridine Ru complexes $Ru(L)(CO)_2X_2$ on silica (e.g., ~1.6% loading of Ru by weight), where the ligand L was either bipyridine or methyl substituted bipyridine and X = Cl, H, SCN, or $COOCH_3$, and obtained activity in the temperature range 100–160 °C. The authors reported enhanced activity when catalysts were activated using a new procedure, that is, by addition of either Na_2CO_3 or NaOH.

The authors concluded that the turnover frequencies for Na_2CO_3 activation were in reasonably good agreement with those from NaOH activation, suggesting that the same catalytically active species was formed in both activation procedures.

Brooks et al. [13, 14] found through combinatorial screening methods a remarkable improvement in Pt/ZrO_2 catalysts for fuel processors for use in fuel cell applications by doping the catalysts with alkali. Over 250,000 experiments were carried out by synthesizing catalyst libraries on 4″ wafers, and screening with a Symyx high throughput scanning mass spectrometer. Among the promising compositions discovered was an important improvement when Pt/ZrO_2 was doped with Na alone or in combination with V. Pigos et al. [15, 16] characterized the catalysts by DRIFTS spectroscopy measurements, and found that formate species were more reactive on the Na doped catalysts. Over Rh/ceria catalysts, Shido and Iwasawa [17] had previously demonstrated that the rate limiting step was C–H bond breaking of formate. Interestingly, Pigos et al. [15, 16] found that formate C–H stretching bands were strongly shifted to lower wavenumbers upon CO adsorption. In transient formate decomposition experiments, both in the presence and absence of steam, Pigos et al. [15, 16, 18, 19] reported that formates over $PtNa/ZrO_2$ decomposed at twice the rate of those observed on Pt/ZrO_2 without Na. Furthermore, in steady state water–gas shift tests, the coverage of formate species was found to be more limited (i.e., by the water–gas shift rate) in DRIFTS for the Na promoted catalysts relative to those without Na. A more comprehensive analysis of Group I alkali promoters was carried also carried out [19], and while Li and K were found to promote the WGS rate, Na was found to provide the greatest benefit. The authors attributed the promoting effect of the alkali dopant to the enhanced reactivity of the formate C–H bond.

Since formate C–H bond scission has been postulated to be the rate limiting step over metal/ceria catalysts [17], it is of interest to return to these catalysts and determine whether a similar promoting effect on the low temperature shift rate can occur as has been found by Honda Research Inc.,

USA for the Pt/ZrO_2 system. To characterize the stability of formate species, Pt/ceria catalysts, doped with Group 1 alkali metals, were probed by infrared spectroscopy of CO adsorption. Steady state and transient water–gas shift tests were carried out using an in-situ DRIFTS cell. Carbonate stability was also assessed by TPD-MS of chemisorbed CO_2.

2 Experimental

2.1 Catalyst Preparation

High surface area ceria was prepared via homogeneous precipitation of the nitrate in urea with aqueous ammonia in a procedure similar to Li et al. [20], whereby urea decomposition is a slow process resulting in a more homogeneous precipitation. Appropriate amounts of $Ce(NO_3)_3 \cdot 6H_2O$ (Alfa Aesar, 99.5%) and urea (Alfa Aesar, 99.5%) were dissolved in 600 ml of deionized water. The mixture was then heated at 90–100 °C with constant vigorous stirring. The precipitate was filtered, washed repeatedly with deionized water, and dried in an oven at 110 °C overnight. The dried precipitate was then crushed and calcined in a muffle furnace at 400 °C for 4 h. Pt was added by incipient wetness impregnation (IWI) of tetraammine platinum (II) nitrate (Alfa Aesar). The resulting catalyst was dried at 110 °C for 24 h, and then calcined at 300 °C for 3 h. The alkali was added by IWI following the calcination using a loading solution containing the corresponding nitrate of Li, Na, K, Rb, or Cs. The catalyst was re-calcined at 300 °C for 3 h. A high alkali doping series was prepared with equivalent atomic loading based on 2.5%Na by weight. Lower alkali-doped catalysts were prepared for Na and K with equivalent atomic loading based on 0.5%Na by weight. A separate, but similar, Pt/ceria catalyst was used as the reference.

2.2 X-ray Diffraction

Powder diffractograms on calcined catalysts were recorded using a PANalytical X = Pert diffractometer, Cu Kα (λ = 0.154 nm) as a radiation source. First, short times were used over a long range to ensure that CeO_2 had formed. The conditions were as follows: scan rate of 0.02°/step, scan time of 1.53 s/step over a 2θ range of 5–90°.

2.3 BET Surface Area

BET surface area measurements were carried out using a Micromeritics Tristar 3000 gas adsorption analyzer. A weight of approximately 0.25 g of sample was used for each test. After being loaded into a Pyrex/Quartz glass cell, the samples were outgassed at 160 °C overnight. Nitrogen adsorption was carried out at its boiling temperature.

2.4 Temperature Programmed Reduction (TPR) and Thermogravimetric Analysis (TGA)

TPR was conducted on unpromoted and platinum promoted ceria catalysts in a Zeton-Altamira AMI-200 unit, which was equipped with a thermal conductivity detector (TCD). Argon was used as the reference gas, and 10%H_2 (balance Ar) was flowed at 30 cm^3/min as the temperature was increased from 50 °C to 800 °C at a ramp rate of 10 °C/min.

2.5 Temperature Programmed Desorption Mass Spectrometry (TPD-MS) of adsorbed CO_2

CO_2 is an important probe molecule for determining the basicity of metal/oxide catalysts [21]. The catalysts were treated in-situ in a Micromeritics AutoChem II 2920 chemisorption analyzer under the following conditions: the samples were first reduced at 300 °C for 8 h using 50 cm^3/min of 10% H_2 in Ar stream. After that, the samples were cooled down to 100 °C in a flowing 50%CO_2 in helium. After flushing with He, TPD was performed in He up to 700 °C, and the ramp rate was 10 °C/min. CO_2 desorbed was measured by a Pfeiffer/Balzers Thermostar mass spectrometer coupled to the Micromeritics system. In order to know the amount of CO_2 desorbed the mass signals were calibrated by using the decomposition of calcium oxalate.

2.6 Diffuse Reflectance Infrared Fourier Transform Spectroscopy (DRIFTS)

A Nicolet Nexus 870 was used, equipped with a DTGS-TEC detector. A high pressure/high temperature chamber fitted with ZnSe windows was utilized as the WGS reactor for in-situ steady state and transient reaction measurements. The gas lines leading to and from the reactor were heat traced, insulated with ceramic fiber tape, and further covered with general purpose insulating wrap. Scans were taken at a resolution of 4 to give a data spacing of 1.928 cm^{-1}. Typically, 256 scans were taken to improve the signal to noise ratio. However, for transient experiments, 32 scans were required. The sample amount utilized was 40 mg.

A steam generator consisted of a downflow tube packed with quartz beads and quartz wool heated by a ceramic

oven and equipped with an internal thermocouple. The lines after the steam addition were heat traced. The steam generator and lines were run at the same temperature as that of the in-situ sample holder of the DRIFTS cell. Water was pumped by a precision ISCO Model 500D syringe pump into a steam generator via a thin needle welded to a 1.6 mm line.

Feed gases (UHP) were controlled by using Brooks 5850 series E mass flow controllers. Iron carbonyl traps consisting of lead oxide on alumina (Calsicat) were placed on the CO gas line. All gas lines were filtered with Supelco O_2/moisture traps. During CO adsorption, the flows were maintained at 3.75 cm^3/min CO and 130 cm^3/min N_2. During water–gas shift testing, 62.5 cm^3/min of the nitrogen balancing gas was replaced by an equivalent flow rate of steam and spectra were recorded until they reached steady state.

2.7 Testing in a Fixed Bed Reactor

Steady state CO conversion measurements were conducted in a fixed bed reactor consisting of a 0.5 in. stainless steel tube with an internal thermocouple. Experiments were conducted using 40 mg of catalyst diluted to 0.4 g with silicon carbide. The catalyst bed was supported on a bed of quartz glass wool. The description of the steam generator, gas delivery system, and ancillary equipment is provided in Sect. 2.6. The conditions were chosen to simulate those of the low temperature shift reactor of a fuel processor, with the exception that CO_2 was not included in the tests. The gas flows were 3.75 cm^3/min CO, 62.5 cm^3/min H_2O, and 67.5 cm^3/min H_2. Catalysts were activated in H_2 (100 cm^3/min at 300 °C) for 1 h prior to reaction testing.

3 Results and Discussion

The ceria prepared was first examined by powder XRD in order to estimate the crystallite domain size. All samples were found to have a crystallite domain size of ~8.4 nm, as determined by line broadening analysis using the integral breadth method with Winfit software (Stefan Krumm 1997). BET results for the calcined catalysts are provided in Table 1. The addition of high alkali doping led to a significant decrease in the BET surface area for all alkali metals. However, the results may be misleading, as they are indicative of the non-activated state of the catalyst, where a high concentration of surface carbonates was observed by infrared spectroscopy. A significant fraction of the carbonates was observed to decompose in infrared spectroscopy after the reduction step. The average pore radius was found to be significantly larger than the reference catalyst, most likely due to blocking of the narrower pores by alkali compounds. When the level of alkali was reduced to 0.5%Na (~0.9% by weight K for an atomic equivalent), the catalysts retained a high fraction of surface area relative to the undoped 2%Pt/ceria catalyst. Furthermore, the average pore radius was virtually identical to the undoped case.

Results of H_2-TPR are depicted in Fig. 1. The unpromoted ceria sample shows that reduction proceeds at two distinct temperatures. The low temperature peak, situated in the range of 450–500 °C, is typically ascribed to reduction of the ceria surface shell [22, 23] involving the removal of surface capping oxygen atoms, while the second peak, at much higher temperature (>700 °C), is assigned to reduction of bulk ceria. As observed in previous investigations [20, 24], addition of metal clusters (e.g., Pt) facilitates the surface reduction step to lower temperatures, while having little impact on the bulk reduction. It has been demonstrated that the reduction of the ceria surface shell is actually a more complicated process, and involves the formation of Type II bridging OH groups associated with the reduced Ce^{3+} defects, as well as the decomposition of carbonate species [24]. The former process can involve H_2 dissociation on the metal and spillover of H to the cerium oxide surface and/or the dissociation of H_2O at the oxygen vacancies [24]. Complicating the reduction of the alkali-doped catalysts is the proposal that the presence of the alkali dopant can hinder the spillover of H· from the Pt to the cerium oxide surface. Similar shifts to higher temperature were observed previously for peaks assigned to the reduction of cobalt oxides when Co/SiO_2 Fischer-Tropsch synthesis catalysts were doped with increasing levels of K [25]. This effect is observed primarily for the case of the higher loaded alkali catalysts (Fig. 1a), where the low temperature reduction peak shifts from ~175 °C for the 2%Pt/ceria catalyst to ~250 °C in the case of the 14.5%Cs doped catalyst, as indicated by the arrow. In the case of the lower alkali-doped samples (Fig. 1b), there is an interesting splitting of the peak, such that the catalyst reduces over a wider range from 75 °C to 210 °C.

The first DRIFTS experiment was to observe if the alkali exerted an impact on the ν(CH) band of the adsorbed formate molecule, as was observed in the case of Pt/ZrO_2 alkali (Li, Na, and K) doped samples by Honda Research Incorporated, USA [15–19]. Figure 2a in combination with Table 2 show that there is a systematic decrease in the band position corresponding to ν(CH) with increasing atomic number of the alkali metal. There are at least two additional bands within the vicinity of the main formate ν(C–H) stretching band. For example, while Binet et al. [26] indicate that the band at ca. 2,950 cm^{-1} corresponds to a coupling of the ν_s(OCO) mode with δ(CH) and that the

Table 1 BET surface area and porosity results

Catalyst	BET SA (m^2/g)	Pore volume (cm^3/g)	Average pore radius (nm)
Reference catalysts			
Ceria	116.4	0.0855	1.47
2%Pt/ceria[a]	110.5	0.0873	1.58
2%Pt/ceria[b]	109.4	0.0862	1.57
Low alkali doping (*equivalent atomic content*)			
2%Pt/0.5%Na/ceria	87.2	0.0670	1.53
2%Pt/0.9%K/ceria	73.7	0.0606	1.64
High alkali doping (*equivalent atomic content*)			
2%Pt/0.8%Li/ceria	15.4	0.0343	4.44
2%Pt/2.5%Na/ceria	9.1	0.0290	6.40
2%Pt/4.3%K/ceria	12.9	0.0286	4.45
2%Pt/9.3%Rb/ceria	7.3	0.0241	6.64
2%Pt/14.5%Cs/ceria	19.6	0.0325	3.32

[a] Reference for high alkali doping series

[b] Reference for low alkali doping series

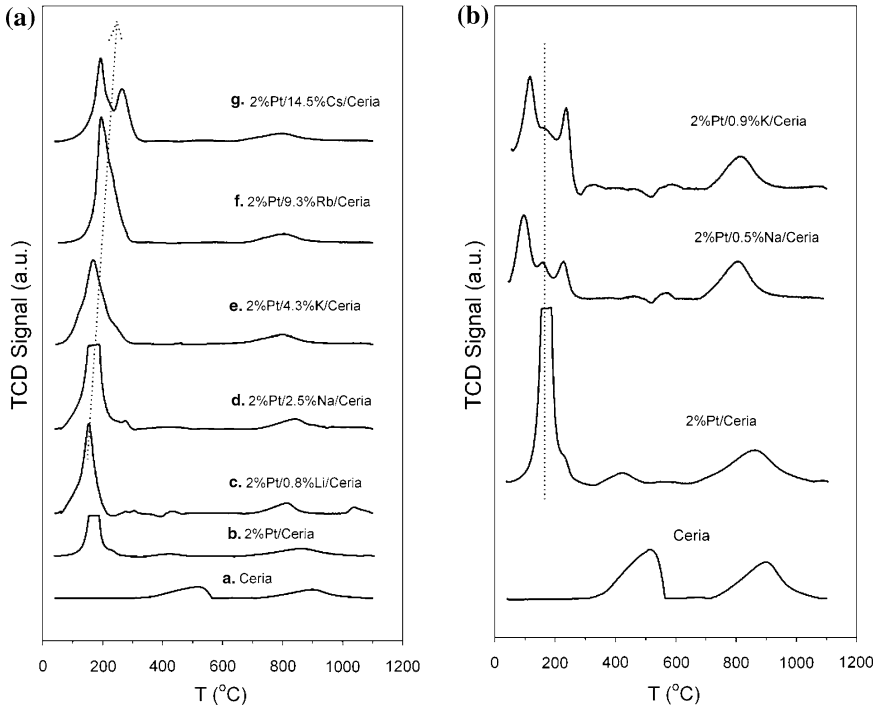

Fig. 1 TPR profiles of (**a**) high alkali-doped Pt/ceria catalysts and (**b**) low alkali-doped Pt/ceria catalysts, relative to the reference catalyst samples

lower wavenumber band at ca. 2,710 cm^{-1} corresponds to 2δ(CH), others have assigned the higher wavenumber band to a ν(CH) band for bridge-bonded formate [27] and the lower wavenumber band to ν(CH) of formaldehyde [28, 29]. In this contribution, we have adopted the assignments of Binet et al. [26], as shown in Table 2. There is clearly a decrease in the band position for 2δ(CH) as a function of the atomic number of the alkali metal present, while the band corresponding to ν_s(OCO) + δ(CH) is not significantly affected. For the higher atomic number alkali metal-doped catalysts, there are additional bands present, either combined within a broadened band or that appear as distinct shoulders on the main band. These may arise due to different degrees of interaction between the alkali promoter and the adsorbed formate molecule. There are a number of competing theories for how the alkali dopant may impact the strength of a bond. First of all, the effect may be geometric in nature, or electronic. Regarding the latter, one common viewpoint in the catalysis literature is that the alkali may interact with a molecule through an

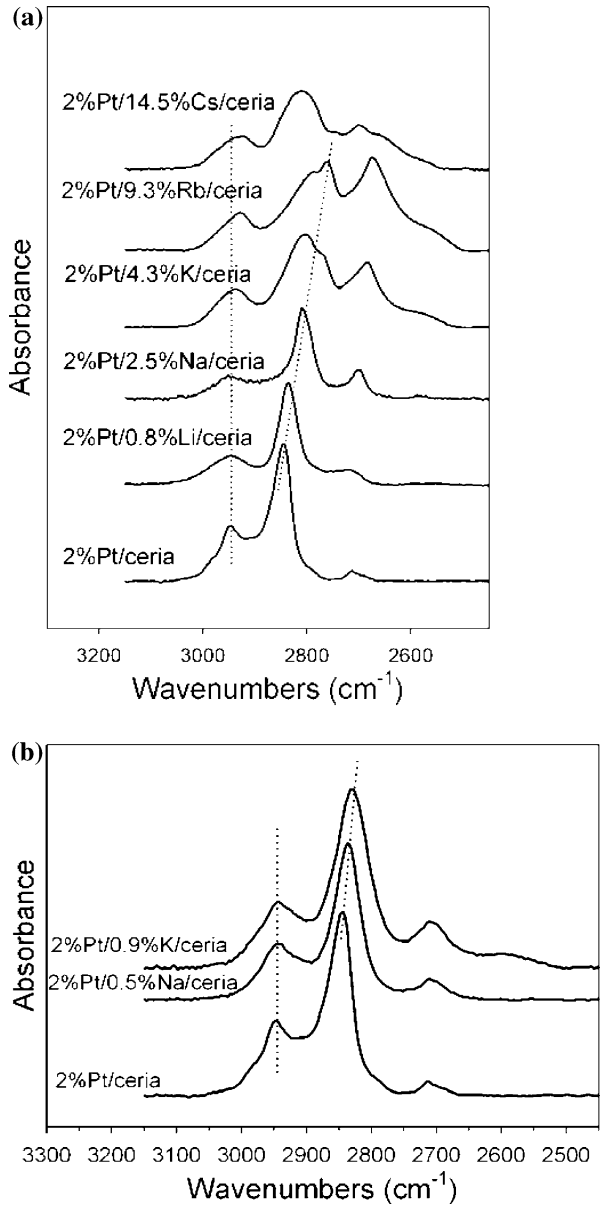

Fig. 2 Formate *v*(CH) band position as a funciton of alkali type for (**a**) high alkali doping and (**b**) low alkali doping

electrostatic force. Ponec [30] found that doping Pt/SiO_2 with K led to an improvement in the *n*-hexane turnover rate during aromatization, and proposed that the alkali could assist in closing the ring of the adsorbed intermediates through an electrostatic effect between the cation and the adsorbed intermediate. In turn, this would accelerate the ring closure turnover rate of the adsorbed intermediate (i.e., in that case, perhaps adsorbed hexatriene). Similarly, it is possible that an electrostatic interaction may induce a weakening of the formate C–H bond, leading to a decrease in the band position. Another common viewpoint is that the alkali can transfer charge [31]. This has also been suggested to occur during aromatization of *n*-hexane over Pt/KL catalysts, where charge transfer from K to the metal may enhance the electron density on Pt. In this case, charge transfer to the ceria component may have an indirect impact on the formate C–H bond. Finally, a third viewpoint is that the presence of the alkali may induce changes in the bonding of the formate to the catalyst surface, such that the formate may change from being bonded in a bidentate manner to another form (e.g., monodentate). This third viewpoint could be electronic or geometric in nature. Whatever the cause, since the rate limiting step of the low temperature water–gas shift reaction over metal/ceria catalysts has been proposed to be due to C–H bond breaking of formate intermediate, the shift of the position of the formate *v*(CH) band as observed in DRIFTS is of considerable interest, as it suggests a weakening of the C–H bond.

Figure 3a and b examine the forward decomposition of the formate species at 130 °C in the presence of H_2O over the alkali-doped catalysts in comparison with the 2%Pt/ceria reference catalyst. It is evident from the Fig. 3a that, while formate is the main species detected upon CO adsorption over each catalyst sample, containing both formate *v*(CH) and asymmetric (i.e., $\sim$1,580 cm^{-1}) and symmetric ($\sim$1,375 cm^{-1}) *v*(OCO) modes [32], the main species following steaming are carbonates. This is clearly the case, as the bands for *v*(CH) decrease to virtually nil while the band positions for *v*(OCO) modes are slightly shifted in position, indicating the formation of a new species. The rate of the formate decomposition appears to be accelerated in the case of the alkali-doped catalysts, especially in the case of the Na, K, Rb, and Cs-doped samples, where the half-life is considerably shortened. The lower absorbance intensity may indicate, however, a decrease in the number of formate molecules adsorbed on the catalyst following CO adsorption. This in turn would suggest that the number of bridging OH groups (active sites) have diminished. Another important finding was that the *v*(CO) bands for adsorbed CO on Pt were very low in intensity compared to the 2%Pt/ceria reference catalyst, suggesting that the alkali was blocking a significant fraction of the Pt surface sites.

For the initial series of catalysts tested with high alkali doping levels, indicated by the light solid lines on Fig. 4, the CO conversion rate was lower relative to the 2%Pt/ceria catalyst. Already, this lower activity may be attributed to the low surface areas of the catalysts, or to the covering of the Pt surface by the alkali and hindering the synergism involved between Pt and ceria in the catalytic mechanism. However, another factor for consideration is the stability of the second proposed intermediate, the carbonate species. Altering the acid-base properties of the catalyst by incorporation of alkali could impact the stability of the adsorbed carbonate species formed from the formate decomposition step of the mechanism.

Table 2 Formate C–H band positions upon CO adsorption at 225 °C using the assignments of Lavalley and coworkers [26]

Catalysts	Band position (cm^{-1})		
	ν(CH)	δ(CH) + ν_S(OCO)	2δ(CH)
Reference catalyst			
2%Pt/ceria	2,844	2,946	2,713
High alkali doping series			
2%Pt/0.8%Li/ceria	2,837	2,947	2,715
2%Pt/2.5%Na/ceria	2,810	2,950	2,700
2%Pt/4.3%K/ceria	2,802 (2,769)	2,952–2,923	2,684
2%Pt/9.3%Rb/ceria	2,760 (2,785)	2,929	2,673
2%Pt/14.5%Cs/ceria	2,809 (2,746)	2,925	2,700 (2,661)
Low alkali doping catalysts			
2%Pt/0.5%Na/ceria	2,837	2,941	2,711
2%Pt/0.9%K/ceria	2,829	2,943	2,711

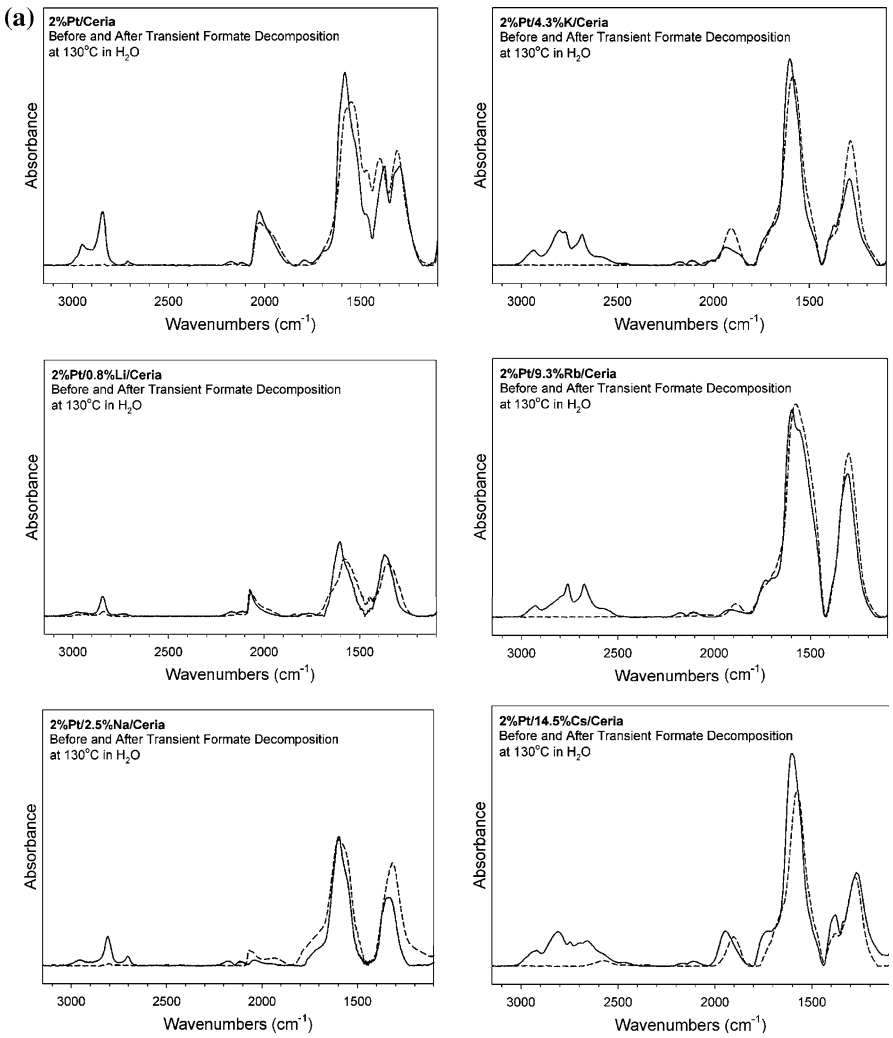

Fig. 3 (**a**) Before and after snapshots of the transient formate decomposition in steam at 130 °C for the heavily alkali doped catalysts with equivalent atomic loading of alkali. Formate is converted to carbonate species. (**b**) Transient formate decomposition in steam at 130 °C for the heavily alkali doped catalysts with equivalent atomic loading of alkali

To explore this hypothesis further, TPD-MS of adsorbed CO_2 was carried out. CO_2 is an acidic molecule and is often utilized to probe the basic sites of metal/oxide catalysts [21]. An added advantage of utilizing CO_2 is that surface carbonates are often considered to be an intermediate in the water–gas shift cycle [17, 24] of metal/ceria catalysts.

Fig. 3 continued

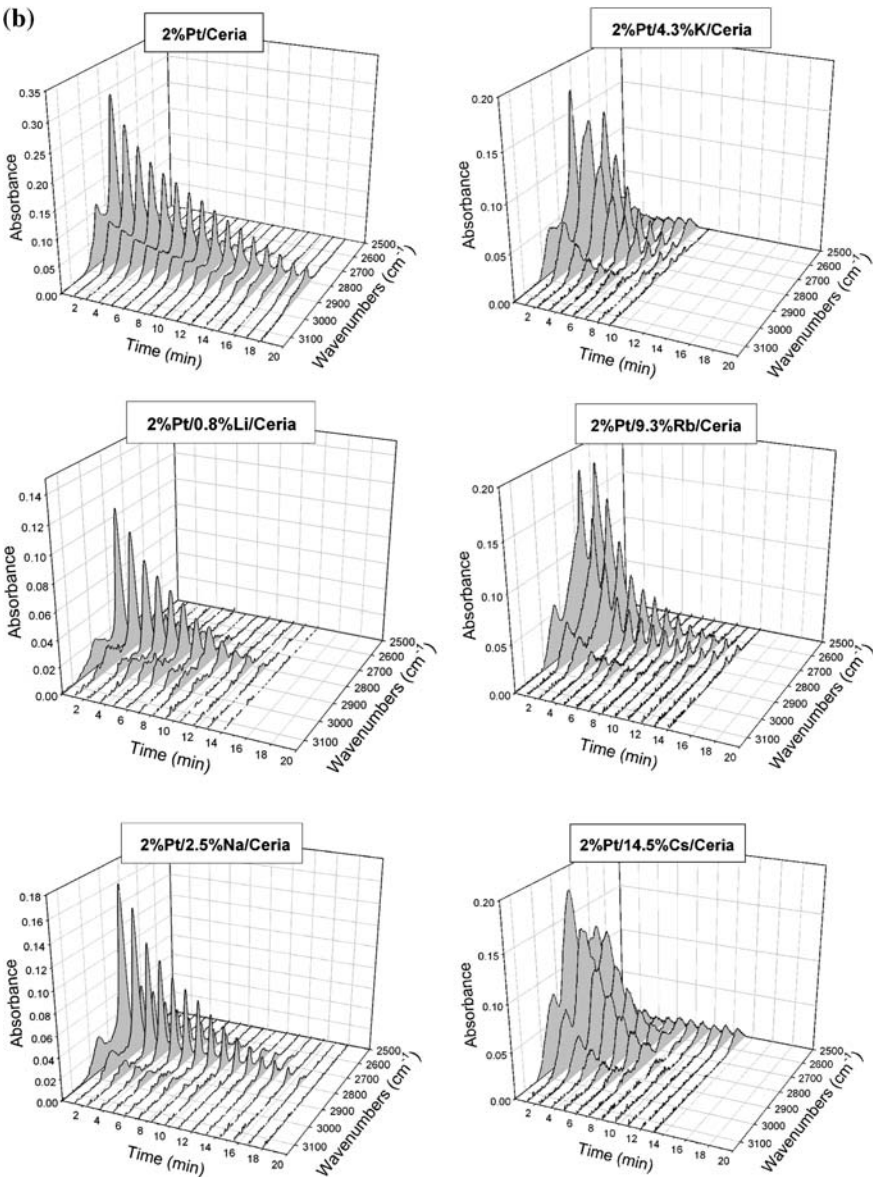

Interestingly, as summarized in Fig. 5a and b and Table 3, the desorption rate of CO_2, and therefore the decomposition rate of the surface carbonate species, is significantly impacted by the alkali type. In a typical profile, two main peaks of interest to the catalysis were evolved—a low temperature peak situated in the temperature range 100–225 °C and a second higher temperature peak in the range of 225–350 °C. Alkali doping altered both the positions of the peak maxima, as well as the absolute and relative amounts of CO_2 desorbed. The peaks were deconvoluted by using a least squares fitting of Gaussian peaks to determine the different contributions to the TPD profiles. A sample fitting is provided in Fig. 5b. In general, as summarized in Table 3, increasing the alkali dopant atomic number led to a decrease in the ratio of the first to second peak, and to an increase in the desorption temperature of the second peak. This characterization suggests an increase in the stability of carbonate species as a function of the alkali atomic number. These results suggest therefore that there may exist a tradeoff between formate stability and carbonate stability from the standpoint of decomposition.

Another testimony to the higher stability of the carbonate species on the alkali-doped catalyst follows from the previous discussion regarding the shift in the temperature of the low temperature peak due to ceria surface reduction. It has been demonstrated previously [24] that contained within this feature is the decomposition of surface carbonates. As shown in the TPR profiles (Fig. 1), the reduction occurring in the low temperature peak is hindered with increasing alkali atomic number. One can

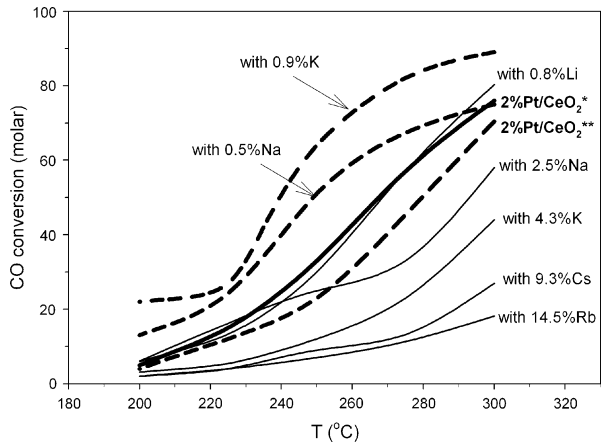

Fig. 4 CO conversion versus temperature during low temperature water–gas shift using a feed containing: 3.75 cm^3/min CO: 62.5 cm^3/min H_2O: 67.5 cm^3/min H_2 (*reference for high alkali doping series; **reference for low alkali doping series)

follow the reduction of the carbonate species using DRIFTS. Single beam intensity spectra are presented in Fig. 6 before and after surface shell reduction. Qualitatively, it appears that the carbonate band intensities over the 2%Pt/2.5%Na/ceria catalyst are higher than those observed for the 2%Pt/ceria reference catalyst, both before and after activation.

The main goal of the investigation was to determine whether a catalyst designer can take advantage of the decreased stability of the formate C–H bond that could lead potentially to higher intrinsic water–gas shift activity through enhanced formate turnover rates achieved by a more rapid C–H bond scission rate. It is clear from the previous discussion that too high a level of alkali doping had been utilized in the initial attempt. Although the formate (i.e., proposed first intermediate [17]) decomposition rate was faster, the CO_2 TPD-MS results suggest that the carbonate (i.e., second intermediate [17]) decomposition rate was impeded.

Therefore, two additional catalysts were prepared with lower alkali loading, one with 0.5% by weight Na and another with an equivalent atomic amount of K (~0.9% loading by weight). Figure 4 shows that these catalysts exhibited even higher water–gas shift activity than the 2%Pt/ceria reference catalyst. CO_2 holdup, found to be problematic with the higher alkali-doped samples, was not deemed to be an issue at the lower alkali doping levels, as characterized by the CO_2 TPD-MS results provided in Fig. 5a (dashed lines). Table 3 indicates that the CO_2 desorption area ratios (i.e., low temperature TPD peak to the high temperature one) were correspondingly higher than those observed for the higher alkali-doped catalysts, and they were also even higher than the ratio observed for the 2%Pt/ceria catalyst. This enhanced ability to desorb

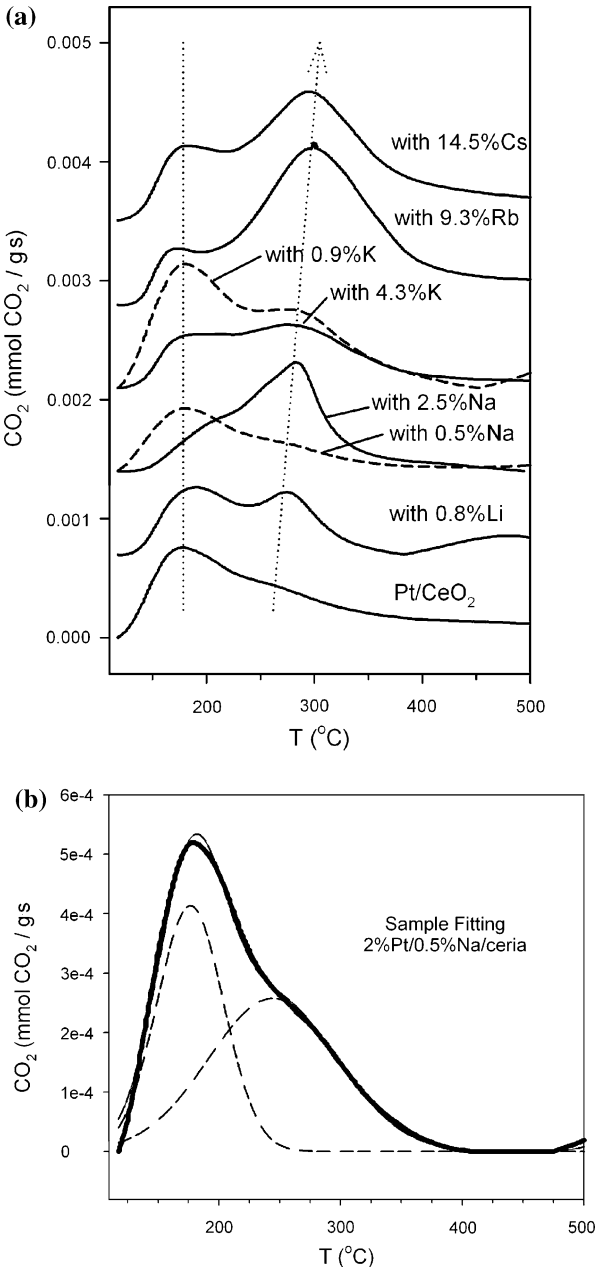

Fig. 5 (**a**) Catalyst first reduced at 300 °C for 8 h. TPD-MS of adsorbed CO_2 with, moving upward, increasing alkali atomic number. (Solid lines) High alkali doping with equivalent atomic content. (Dashed) Low alkali doping with equivalent atomic content. (**b**) Sample Gaussian fitting of the CO_2 TPD peaks for 2%Pt/0.5%Na/ceria

CO_2 relative to the higher alkali doped catalysts, may be the result of a promoting effect of Pt to assist in the decomposition of carbonate. With the lower alkali doping levels, Fig. 7a suggests that Pt is not significantly covered by alkali, as indicated by the high intensities of the ν(CO) bands for adsorbed CO on Pt (Fig. 7a, right side). ν(CO) bands for adsorbed CO on Pt displayed an asymmetric character, most likely due to the presence of both linear and

Table 3 TPD-MS of adsorbed CO_2. Characterization of carbonate stability defined in terms of major peak positions and ratio of low to high temperature peaks

Catalyst	T_1 (°C)	T_2 (°C)	Area 1	Area 2	Area 1/Area 2
Reference catalyst					
2%Pt/ceria	175.8	242.4	0.0338	0.0568	0.59
High alkali doping series					
2%Pt/0.8%Li/ceria	188.2	270.7	0.0373	0.0420	0.89
2%Pt/2.5%Na/ceria	214.1	279.7	0.0280	0.0484	0.58
2%Pt/4.3%K/ceria	167.5, 194.0	272.9	0.00597, 0.01005	0.0766	0.21
2%Pt/9.3%Rb/ceria	176.5	298.3	0.0229	0.166	0.14
2%Pt/14.5%Cs/ceria	182.3	293.3	0.0358	0.132	0.27
Low alkali doping catalysts					
2%Pt/0.5%Na/ceria	176.5	244.4	0.0279	0.0340	0.82
2%Pt/0.9%K/ceria	178.2	267.3	0.0585	0.0922	0.63

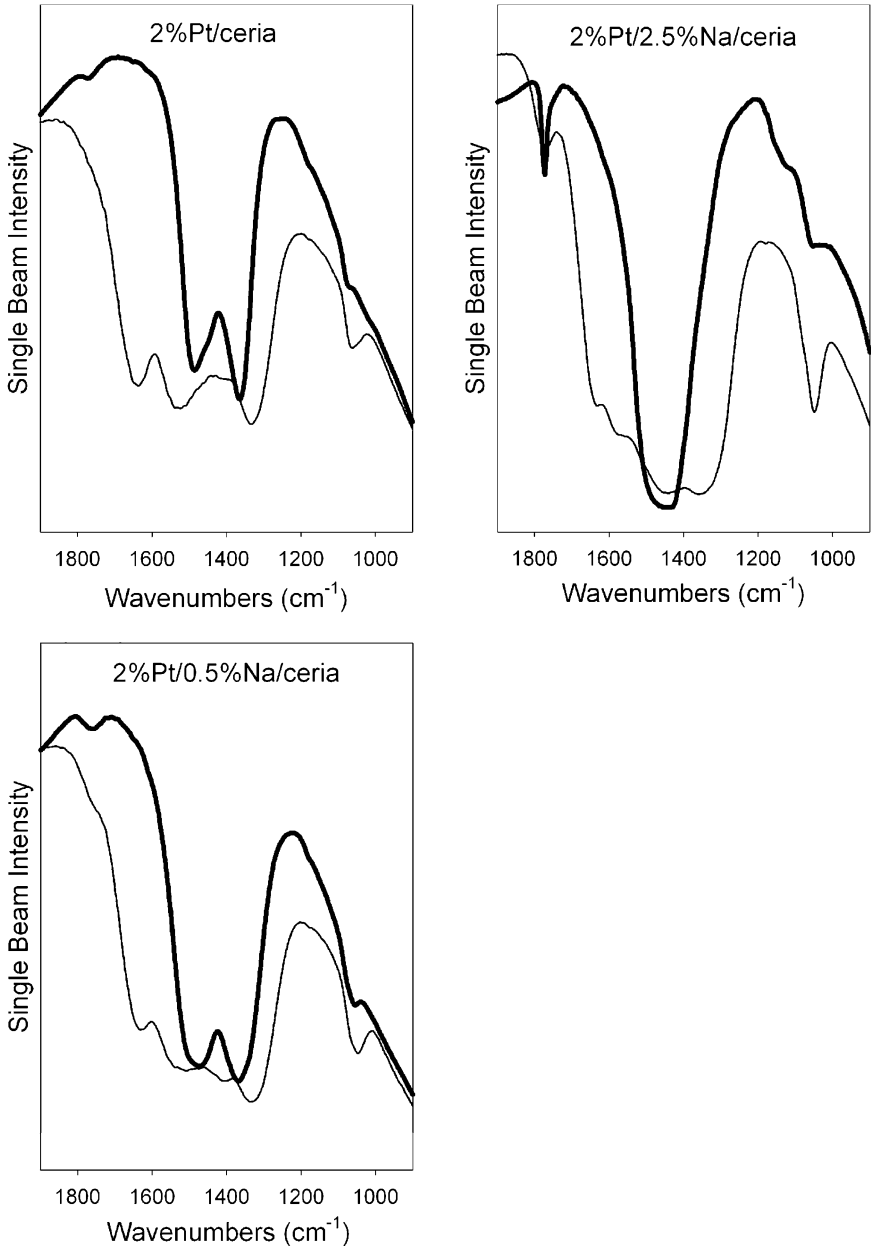

Fig. 6 Infrared single beam spectrum (light) before and (heavy) after reduction in hydrogen at 300 °C for (upper left) 2%Pt/ceria, (upper right) 2%Pt/2.5%Na/ceria, and (lower) 2%Pt/0.5%Na/ceria

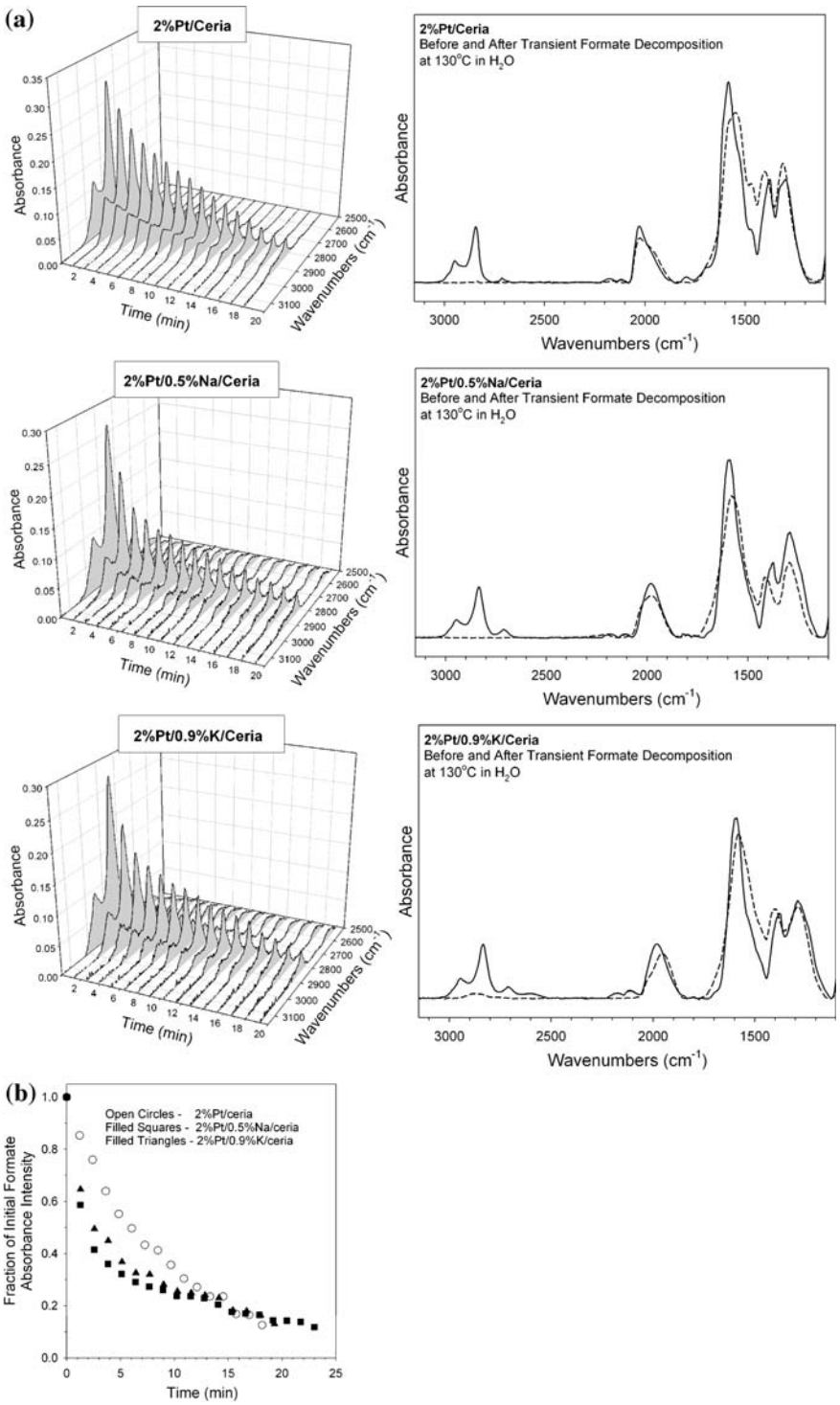

Fig. 7 (**a**) (left) Transient formate decomposition in steam at 130 °C for the lower loading alkali doped catalysts with equivalent atomic loading of alkali. (right) Before/after snapshots. (**b**) Transient formate decomposition in steam at 130 °C for the lower loading alkali doped catalysts with equivalent atomic loading of alkali, including (filled squares) 2%Pt/0.5%Na/ceria and (filled triangles) 2%Pt/0.9%K/ceria, in comparison with the reference 2%Pt/ceria catalyst (open circles)

bridge-bonded CO. Interestingly, the maximum for these asymmetric bands displayed a shift in the peak maximum from $\sim$2,030 cm^{-1} for the 2%Pt/ceria reference catalyst, to $\sim$1,980 cm^{-1} for the Na and K doped catalysts. This may be the result of a decrease in the linear to bridge (L/B) ratio [33] as has been observed after doping non-acidic supported Pt aromatization catalysts with K, perhaps due to an electronic effect as previously described [31]. TPR results, also described previously and depicted in Fig. 1, are in line with this conclusion, as the peaks (on average) are found to be at a lower temperature for the surface reduction of ceria than for the higher alkali-loaded samples. Furthermore, Fig. 6 demonstrates that the carbonates on the lower alkali doped catalyst (2%Pt/0.5%Na/ceria) are

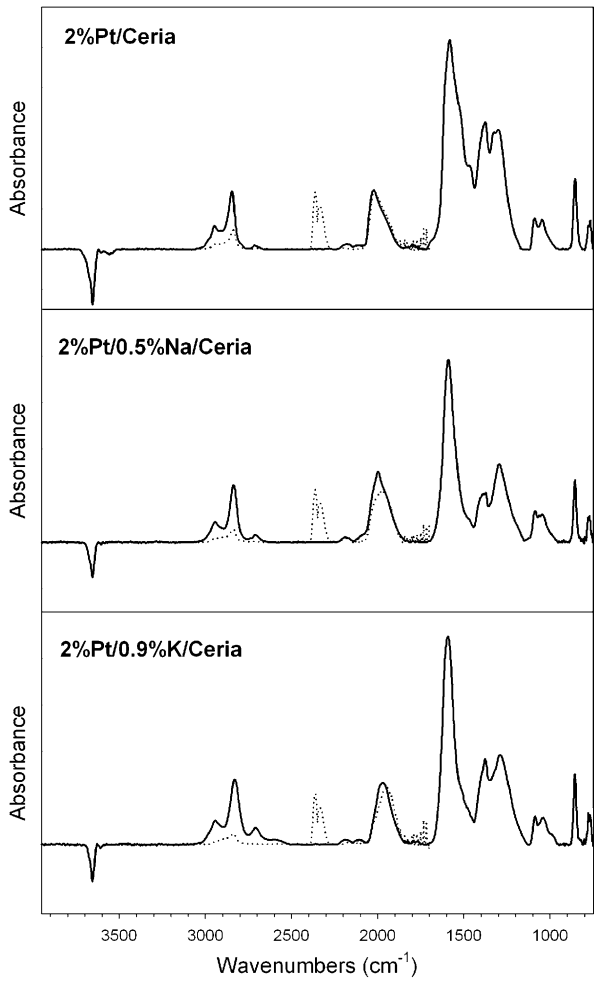

Fig. 8 (bold) DRIFTS of CO adsorption over partially reduced catalysts. (dotted) DRIFTS response of formate to steady state water–gas shift feed at 225 °C using $CO:H_2O:N_2$ feed

similar in shape and intensity (both before and after reduction) to those species found on 2%Pt/ceria relative to the carbonates observed on the higher alkali-doped sample (2%Pt/2.5%Na/ceria), which displayed higher absorption intensity.

Figure 2b shows that the formate bands, though not as significantly shifted in position as compared to the higher alkali-doped catalysts, are still shifted to lower wavenumbers. In transient formate decomposition tests depicted in Fig. 7a (left), the formates clearly decompose at a faster rate (compare initial spectra). Figure 7b shows the change in absorbance relative to the initial formate spectrum as a function of time for each catalyst during transient decomposition in steam at 130 °C. The 1/3-lives of the forward formate decomposition for the alkali-doped catalysts (~4.7 min for 0.5%Na and ~6.2 min for 0.9%K) are much shorter in comparison with that of the 2%Pt/ceria reference catalyst (~10.2 min). Again, the resulting species formed from the formate decomposition are carbonate species, as indicated by the dashed line spectra on the right side of Fig. 7A (right). The dashed spectra indicate that the formate ν(CH) band has disappeared, and the ν(OCO) asymmetric and symmetric bands are shifted in position, suggesting the formation of new chemical species.

One final comparison of interest for these catalysts is the relationship between the formate decomposition rate and the CO conversion rate during low temperature water–gas shift. First, CO adsorption is used to probe the active Type II bridging OH groups to generate formate bands. That is, the formate band intensity is indicative of the total number of active available Type II bridging OH group active sites. Figure 8 shows that when N_2 balancing gas using during CO adsorption is switched to steam, the formate coverage becomes limited by the water–gas shift rate, most likely due to the turnover of the formate intermediate. Figure 8 indicates that the formate coverage is even more limited during steady state water–gas shift for the alkali-doped catalysts relative to the undoped 2%Pt/ceria reference catalyst (Fig. 8, top). This suggests that the formate is reacting faster over the alkali-doped catalysts. Using the 2%Pt/ceria catalyst as a reference, Table 4 demonstrates that the ratio of formate coverages between catalysts, a relative measurement of the formate turnover rates, is very similar to that of the ratio of the CO conversion rates between catalysts. This strongly suggests that the formate intermediate is the main intermediate of interest for water–gas shift. The study demonstrates that increases in catalyst activity can be made by focusing on ways to weaken the formate C–H band, as its scission is the proposed rate limiting step of the low temperature water–gas shift cycle.

4 Conclusions

The promotion of Pt/ceria catalysts with alkali metals is an optimization problem. The presence of the alkali promoter

Table 4 Comparison of the ratio of formate coverages with the ratio of the CO conversion rates during water–gas shift at 225 °C for the lower alkali loaded catalysts relative to the non-alkali doped Pt/ceria catalyst (ID #1)

ID#	Catalyst	$\theta_{formate}$	$\theta_{formate,\ 1}/\theta_{formate,\ i}$	X_{CO}	$X_{CO,\ i}/X_{CO,\ 1}$
1	2%Pt/ceria	0.27	1	15.0	1
2	2%Pt/0.5%Na/ceria	0.20	1.4	24.3	1.6
3	2%Pt/0.9%K/ceria	0.11	2.2	27.0	1.8

leads to an important weakening of the formate C–H bond, as demonstrated by a shift to lower wavenumbers of the ν(CH) vibrational mode. However, with increasing alkalinity, the stability of the second adsorbed intermediate, carbonate, which is formed as a direct result of the formate decomposition step, increases. Evidence of this was obtained by TPD-MS of adsorbed CO_2 probe molecule. In addition, increasing the amount of alkali to too high a level leads to other negative factors, including decreased BET surface area, blocking of the Pt surface sites, and a shift in the temperature of the surface shell reduction step of ceria. As a result, if the alkalinity is too high, the CO conversion rate during water–gas shift decreases.

At lower levels of alkali, however, it was demonstrated that the negative factors previously mentioned can be avoided such that one may take advantage of the weakening of the formate C–H bond and improve the overall turnover frequency during water–gas shift. This was demonstrated at 0.5%Na and 0.9%K doping levels. The formate turnover rate was measured by both transient and steady state DRIFTS measurements and found to increase significantly. A corresponding increase in the CO conversion rate during low temperature water–gas shift was observed.

Acknowledgment The work was sponsored by the Commonwealth of Kentucky.

References

1. Sato S, White JM (1980) J Am Chem Soc 102:7206
2. Wagner FT, Somorjai GA (1980) J Am Chem Soc 102:5494
3. Sato S, White JM (1981) J Catal 69:128
4. Vedage GA, Pitchai R, Herman RG, Klier K (1984) Proc. 8th Internat. Congress on Catal., Berlin, Germany, p 47
5. Klier K (1992) Catal Today 15:361
6. Campbell CT, Koel BE, Daube KA (1987) J Vac Sci Technol A 5:810
7. Campbell JM, Nakamura J, Campbell CT (1992) J Catal 136:24
8. Basinska A, Domka F (1993) Catal Lett 17:327
9. Basinska A, Domka F (1997) Catal Lett 43:59
10. Jozwiak WK, Basinska A, Goralski J, Maniecki TP, Kincle D, Domka F (2000) Stud Surf Sci Catal 130:3819
11. Luukkanen S, Homanen P, Haukka M, Pakkanen TA, Deronzier A, Chardon-Noblat S, Zsoldos D, Ziessel R (1999) Appl Catal 185:157
12. Luukkanen S, Haukka M, Kallinen M, Pakkanen TA (2000) Catal Lett 70:123
13. Brooks CJ, Hagemeyer A, Yaccato K, Carhart R, Herrmann M (2005) 19th North Am. Catal. Soc. Meeting, May 22–27, Philadelphia, Pennsylvania, USA
14. Yaccato K, Carhart R, Hagemeyer AG, Herrmann M, Lesik A, Strasser P, Turner H, Volpe1 AF, Weinberg H, Brooks CJ (2006) AIChE Spring National Meeting April 23–27, 2006, Orlando, FL
15. Pigos JM, Brooks CJ, Jacobs G, Davis BH (2006) Prepr Am Chem Soc Div Pet Chem
16. Pigos JM, Brooks CJ, Jacobs G, Davis BH (2006) Evidence of enhanced LTS water–gas shift rate with Sodium promoted Pt-ZrO_2-based catalyst discovered by combinatorial methods, AIChE Annual Meeting abstract
17. Shido T, Iwasawa Y (1993) J Catal 141:71
18. Pigos JM, Brooks CJ, Jacobs G, Davis BH (2007) Appl Catal A: General 319:47
19. Pigos JM, Brooks CJ, Jacobs G, Davis BH Appl Catal A: General, (in press)
20. Li Y, Fu Q, Flytzani-Stephanopoulos M (2000) Appl Catal B 27:179
21. Lavalley JC (1996) Catal Today 27:377
22. Yao HC, Yu Yao YF (1984) J Catal 86:254
23. Laachir A, Perrichon V, Badri A, Lamotte J, Catherine E, Lavalley JC, El Fallah J, Hilaire L, Le Normand F, Quemere E, Sauvion GN, Touret O (1991) J Chem Soc Faraday Trans 87:1601
24. Jacobs G, Graham UM, Chenu E, Patterson PM, Dozier A, Davis BH (2005) J Catal 229:499
25. Jacobs G, Das TK, Zhang Y, Li J, Racoillet G, Davis BH (2002) Appl Catal A: General 233:263
26. Binet C, Daturi M, Lavalley JC (1999) Catal Today 50:207
27. Shido T, Iwasawa Y (1992) J Catal 136:493
28. Li C, Sakata Y, Arai T, Domen K, Maruya KI, Onishi T (1989) J Chem Soc Faraday Trans I 85:1451
29. Tabakova T, Boccuzzi F, Manzoli M, Idakiev V, Andreeva D (2003) Appl Catal A: General 252:385
30. Fukunaga T, Ponec V (1997) Appl Catal A: General 154:207
31. Larsen G, Haller GL (1989) Catal Lett 3:103
32. Holmgren A, Anderson B, Duprez D (1999) Appl Catal B 22:215
33. Mojet BL, Miller JT, Koningsberger DC (1999) J Phys Chem B 103:2724